

Molecular Dynamics Simulation Study of the effect of temperature and strain rate on the Elastic Properties of bimetallic Nanowires.

Subramanian K.R.S. Sankaranarayanan, Venkat R. Bhethanabotla and Babu Joseph*

Sensors Research Laboratory, Department of Chemical Engineering,

University of South Florida, Tampa, Florida, 33620, USA.

Abstract:

Nanomaterial sensing layers are employed for chemical and biological species detection in surface acoustic wave (SAW) sensors. The response characteristics of these sensors depend on the changes in the mechanical properties of the nanomaterials as the SAW propagates through the sensing layer. Knowledge of the mechanical properties is important to establish the stability and robustness of SAW sensors. In this paper, we investigate the mechanical properties of bimetallic nanowires which are a class of nanomaterials used in SAW sensors.

Molecular dynamics (MD) simulation of infinitely long, cylindrical bimetallic Pd-Pt nanowires, with an approximate diameter of 1.4 nm and varying compositions (25 and 50% Pt) are used to investigate its mechanical properties. The nanowires are subjected to uniaxial tensile strain along the [001] axis. The empirical quantum Sutton-Chen potential function is used to describe the inter-atomic potential between the various transition metal atoms. A loose-coupling thermostat (Berendsen) is selected for finite-temperature control of the simulated system, with a time constant of 25% of the total relaxation time during each strain increment. Previous studies have established that the low temperature stable phases of 25 and 50% Pt nanowires exhibit hcp and fcc crystal type, respectively². In the present simulation, these nanowires are subjected to varying strain rates of 0.05%, and 5.0% ps⁻¹, at simulation temperatures of 50 and 300 K, in order to study the effects of different strain rates and thermal conditions on the deformation characteristics and mechanical properties of the nanowire. Analyses of the changes in crystal structure associated with the wire deformation were used to deduce its mechanical properties. Comparisons with the behavior exhibited by pure Pd and Pt nanowires of similar diameter were also carried out in the present study.

The mechanism of stress-strain response is investigated under various loading conditions. At low temperature and strain rate, where crystal order and stability are highly preserved, the calculated stress-strain response of pure Pt and Pd as well as Pd-Pt alloy nanowires showed clear periodic, stepwise dislocation-relaxation recrystallization behavior. Crystalline to amorphous transformation takes place at high strain rates (5% ps⁻¹), with amorphous melting detected at 300 K. Due to higher entropy of the nanowire at higher temperature and strain rate, periodic stress-strain behavior is absent, and superplasticity behavior is observed. Deformation of nanowires at higher strain rates and low temperature, when the superplasticity characteristic is significantly enhanced, results in the development of a single-walled helical structure. We find that the Young's modulus of both the single component as well as alloy nanowires depends on the applied strain rate and is about 70-85% of the bulk value depending on the alloy composition. The Poisson ratio of Pd rich alloys is 60-70% of its bulk value whereas that of Pt rich alloys is not significantly changed at the nanoscale. The influence of the changes in mechanical properties of nanowires on their applicability in sensors and other areas are also discussed. The results are expected to confirm the higher mechanical stability exhibited by Pd-Pt nanowire alloys of certain composition range over pure Pd and Pt nanowires.

* Corresponding author. Electronic address: venkat@eng.usf.edu

I. Introduction

Nanowires represent structures having multifunctional potential and have been the focus of intense research primarily due to their unusual mechanical, thermal and electrical properties. The unique properties of nanowires result from their finite size and help them find applications in many different areas such as catalysis, sensing, microelectronics, etc. The knowledge of mechanical properties of nanowires is important for emerging applications such as nanocomposite strengtheners, nanoscale interconnects and active components in nanoelectromechanical (NEMS) devices.

The search for nanomaterials having a combination of desirable properties such as high mechanical strength, reversible inelastic deformation, fatigue resistance and the ability to act as sensors and actuators has intensified in recent years. Nanowires made of Pd and its alloys are employed for chemical and biological species detection in surface acoustic wave (SAW) sensors. The propagation of SAW results in these nanowires being subjected to continuous stresses. Knowledge of the mechanical properties of these nanowires is therefore important in establishing the stability and robustness of nanomaterial based SAW sensors.

Experimental work based on the scanning tunneling microscopy (STM) and atomic force microscopy (AFM) and related techniques have been used to study stress-strain relationship in nanowires. In these experiments, the tip of the STM or AFM is brought sufficiently close to the substrate at elevated temperatures and a whisker of material is drawn. The length of the whisker drawn before breaking occurs depends on the elastic property of the material. The force acting between the tip of the STM or AFM and the substrate can be measured and the resulting high resolution stress-strain plots can be analyzed to understand the mechanical behavior of thin wires. It has been found that the properties strongly depend on the temperature, nature of the material involved as well as the dimensions of the sample.

Computer simulations such as molecular dynamics (MD) represent a form of numerical experiments which can be used to complement laboratory studies based on STM or AFM. Atomistic simulations at the nanoscale have shown that surface stresses and crystallographic orientation play a dominant role in characterizing material properties^{1, 2}. The effects of intrinsic surface stresses have been found to endow nanowires with extremely high yield stresses and strain^{3, 4}, as well as yield strength asymmetry in tension and compression. Similarly, crystallographic orientations have been shown to have a direct, first order effect on the deformation mode in fcc nanowires⁵.

Most of the MD simulations have focused on single component metals. In particular, analysis of tensile failure modes in metal nanowires under different orientations has received greater attention. Zhang et al. studied the structure and properties of Ni nanowires. Koh et al. studied temperature and strain rate effects on solid platinum nanowires subjected to uniaxial tension⁶. Several such studies on gold nanowires are also available⁷⁻⁹. These demonstrate the ability of gold nanowires to form single atomic chains under tensile loadings. Stress driven phase transformation from fcc to bct (body-centered tetragonal) in gold nanowires was observed by Diao et al^{10, 11}. Similarly, stress induced phase transformation in inter-metallic Ni-Al nanowires was reported by Park¹². Shape memory and pseudo-plastic behavior were observed in single crystalline monatomic fcc nanowires¹³. Gonzalez et al. studied structural and quantum conductance properties of atomic size Cu nanowires generated by mechanical stretching¹⁴. Ikeda et al. used Finnis-Sinclair potentials to study strain induced amorphization in Ni and Ni-Cu alloys¹⁵.

Although many studies have focused on single component systems such as gold, nickel and copper nanowires, few studies have been dedicated to the study of mechanical properties of alloy nanowires. Complex phenomena such as surface segregation and micro-mixing occur in alloys of finite-sized structures such as nanowires. For a given composition of the bimetallies, the microstructure is dictated by surface energies and mixing energies of the constituent atoms. Atoms with lower surface energies tend to segregate to low coordination number sites, the extent of which is determined by the interplay between surface energies, mixing energies and entropy. Available experimental and theoretical evidence suggest a strong dependence of mechanical properties of nanowires on alloy composition and microstructure. The objective of this study is to investigate this dependence using MD simulation.

Specifically, we study the effect of strain rate and temperature on the mechanical properties of bimetallic Pd-Pt nanowires using MD simulations employing quantum Sutton-Chen potential function for two representative Pd compositions i.e. 25% and 50% Pt.

II. Initial nanowire size and configuration

All the transition elements including Pd and Pt exhibit an fcc structure in the bulk solid phase. A large block of fcc was formed from a fcc unit cell by replicating in ABC directions. Using various cutoff radii, cylindrical structures representing nanowires of different diameters (D) having approximately 1.4 nm were created. The nanowires were modeled as infinitely long wires by the application of periodic boundary condition along the wire axis. By choosing different length/diameter ratios, it was ensured that the results were not influenced by the periodic boundary conditions for the simulated infinitely long nanowires.

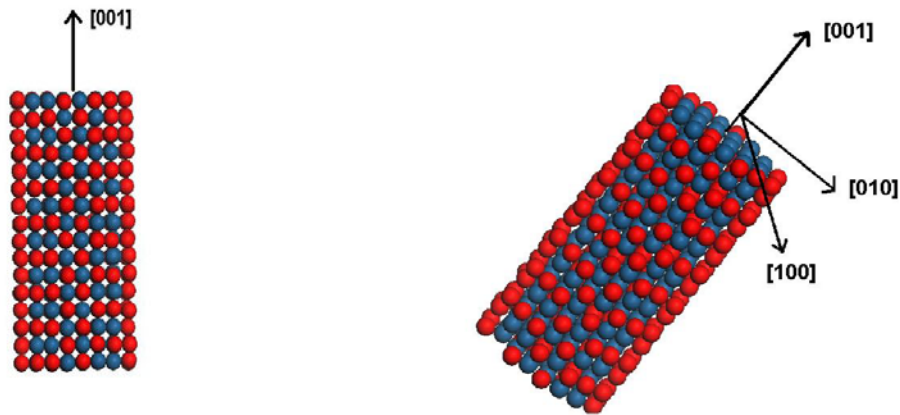


Figure 1. $(\text{Pd}_{0.5}\text{-Pt}_{0.5})$ nanowire having 16 atomic layers (416 atoms) in its initial unstressed state. Pd atoms are shown in red whereas Pt atoms are represented in blue.

To identify the initial atomic positions of the constituent atoms for a given composition of the bimetallic, these structures were subjected to a Metropolis Monte-Carlo simulation employing a bond order simulation (BOS) model, to generate the minimum free energy initial configuration which was subsequently used for studying the stress-strain response. The BOS model has been tested over a range of bimetallics and comparisons with experimental data reveal close agreement with the microstructure predicted by the BOS model. Although Monte-Carlo simulations employing Sutton-Chen potential have also been used to predict the global minima of transition clusters, our calculations indicate that the equilibrium structures obtained using BOS model are more energetically stable compared to those obtained using Sutton-Chen potential model.

III. Computational details

2.1 Potential function

Molecular Dynamics (MD) simulations using DLPOLY were performed to gain insights into the melting process and thermal properties at the atomistic level. All the thermodynamic and transport properties were obtained as time averages over the particle positions and velocities. The embedded atom potential and other long range potentials like the Sutton-Chen potential based on Finnis-Sinclair type of potentials have been used in the literature successfully to predict the thermal and mechanical properties of fcc based metals such as Pd and Pt. The local electronic density is included to account for the many body terms.

Based on the Sutton-Chen potential, the potential energy of the finite system is given by,

$$U_{tot} = \sum_i U_i = \sum_i \epsilon \left[\sum_{j \neq i} \frac{1}{2} V(r_{ij}) - c \rho_i^{1/2} \right] \quad (3.1)$$

Here, $V(r_{ij})$ is a pair potential to account for the repulsion resulting from Pauli's exclusion principle.

$$V(r_{ij}) = \left(\frac{a}{r_{ij}} \right)^n \quad (3.2)$$

The local density accounting for cohesion associated with any atom i is given by,

$$\rho_i = \sum_{j \neq i} \phi(r_{ij}) = \sum_{j \neq i} \left(\frac{a}{r_{ij}} \right)^m \quad (3.3)$$

The Sutton-Chen potential predicts properties involving defects, surfaces and interfaces poorly. The Quantum Sutton-Chen potential (hereafter referred to as QSC), includes quantum corrections and takes into account the zero point energy allowing better prediction of temperature dependent properties. The QSC parameters for the Pd and Pt are listed in Table 1. The geometric mean was used to obtain the energy parameter ϵ and the arithmetic mean was used for the remaining parameters, to predict the nature of interaction between Pd and Pt.

Table 1. Potential parameters used in MD simulations for Pd-Pt nanowires

Quantum Sutton-Chen	N	M	E (eV)	C	a(Å)
Pd	12	6	3.2864e-3	148.205	3.8813
Pt	11	7	9.7894e-3	71.336	3.9163

Differentiating Eq. (3.1) with respect to r_{ij} , the total force of the system is given by:

$$F_{QSC} = -\frac{\epsilon}{r_{ij}} \sum_{j \neq i} \left[n \left(\frac{a}{r_{ij}} \right)^n - \frac{mc}{2} (s_i^{-1/2} + s_j^{-1/2}) \left(\frac{a}{r_{ij}} \right)^m \right] \hat{r}_{ij} \quad (3.4)$$

In the above expression, \hat{r}_{ij} is the unit vector representing inter-atomic distance between atoms i and j . The parameter s_i is a pairwise additive potential that accounts for the electronic repulsion arising from Pauli's

exclusion principle and is given by $s_i = \sum_{\substack{j=1 \\ (j \neq i)}}^N \left(\frac{a}{r_{ij}} \right)^m$.

2.2 MD Simulation details

The MD simulations were carried out in an ensemble approximating the canonical with a constant number of atoms N and volume V with periodic boundary condition applied along the nanowire axis. The equations of motion were integrated using velocity-Verlet algorithm. The atomic velocities were scaled against the simulation temperature using Berendsen thermostat. The simulated strain rate is given as:

$$\dot{\epsilon} = \frac{\Delta \epsilon_{zz}}{N_{step} \Delta t} \quad (3.5)$$

where, $\epsilon_{zz} = \frac{L_z(N_{step}) - L_z(0)}{L_z(0)}$ represents the nominal strain of the nanowire at each time-step. The

strain increment at each step was fixed at 0.5% per increment. The number of relaxation steps (N_{step}) was fixed at 10000. By varying the time-step of the simulation (Δt) from 0.01 fs to 1 fs, different strain rates ranging from 5% ps⁻¹ to 0.05% ps⁻¹ were simulated. The Berendsen thermostat with a coupling constant of $\tau=0.025, 0.25$ and 2.5 ps was used for the respective strain rates. These resulted in modest temperature fluctuations, which lead to correct canonical averages of the system properties. The system properties during each strain increment were computed by averaging over the final 2000 steps. The axial stress was computed as the arithmetic mean of the local stresses on all the atoms:

$$\sigma_{zz}(\epsilon) = \frac{1}{N\Omega^i} \sum_{i=1}^N \sum_{\substack{j=i \\ j \neq i}}^N F_{ij}^z(\epsilon) r_{ij}^z(\epsilon) \quad (3.6)$$

In the above equation, F_{ij}^z represents (001) component of the pair-wise inter-atomic force between atoms i and j , obtained from Eq. (3.6). Ω^i refers to volume of atom i and r_{ij}^z represents inter-atomic distance along the (001) direction between the ij pair. The stress-strain responses (Eq. (3.6)) as well as elastic properties such as Young's Modulus and Poisson's ratio of nanowire obtained from the simulation statistics are analyzed in the subsequent sections.

IV. Results

The simulated stress-strain response of Pd, Pt and their alloys under various loading conditions is presented in this section. The temperatures at which the response was studied were well below the surface melting temperatures of the nanowires. This ensured that the starting configurations of nanowires were completely solid phase. In the present study, we have used various potential cutoff values (for generation of Verlet neighbor list) between 2-2.5 times lattice constant for each temperature and strain rate and found that the results obtained are independent of the same.

1. Mechanism of stress-strain response in nanowires under low strain rate conditions

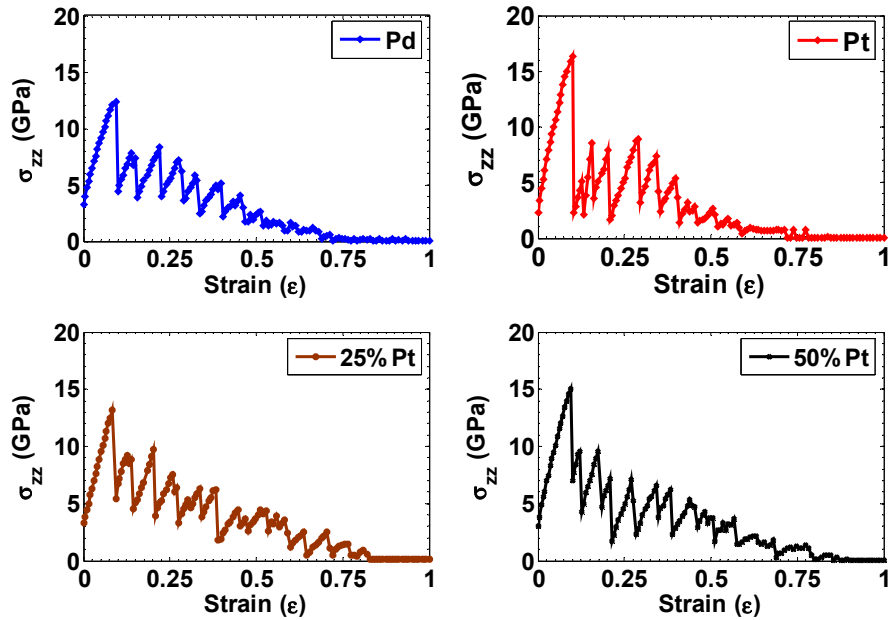
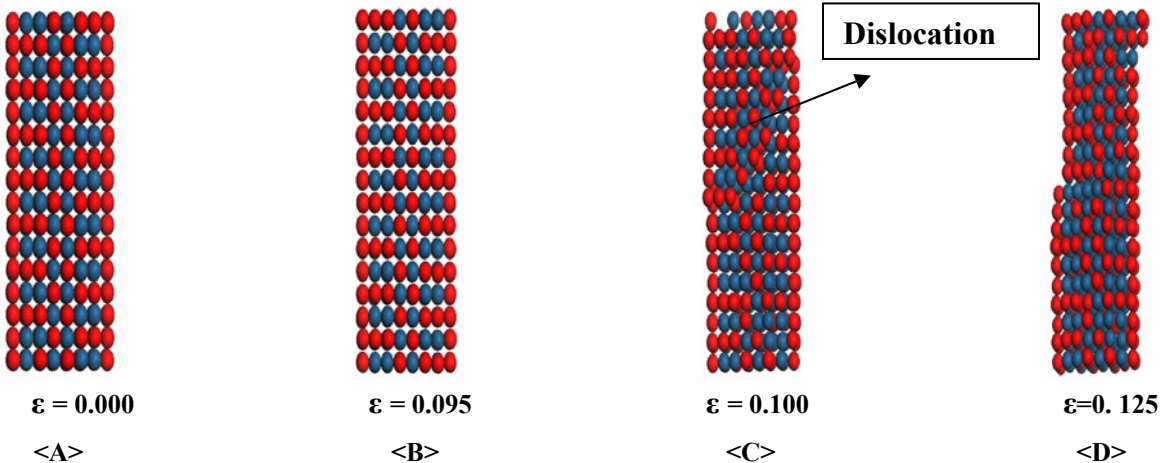


Figure 2. Stress-Strain response of alloy nanowires at $T=50$ K and strain rate= $0.05\%/ps$.

The stress-strain response starting from an initial unstressed state to complete rupture for Pd, Pt as well as their alloy nanowires simulated at 50 K and 0.05%/ps strain rate are shown in Fig. 2. All the materials respond to the strain in qualitatively the same way. The nanowire extension commences with an elastic deformation from its initial state <A> to its threshold value defined as the first yield state . At these low strains, the stress is related to strain by Hooke's law. For 50% Pd alloy nanowires, the first yield strain (ϵ_{fy}) corresponds to 0.095 and the corresponding stress (σ_{fy}) is 15.03 GPa. Beyond the first yield state, the wire experiences an abrupt dislocation and undergoes an irreversible structural rearrangement to a reconstructed crystal configuration shown in <C>. The nanowire at undergoes slippage along the (111) plane which results in a nearly discontinuous drop in the stress value. For a closed pack structure such as fcc, the smallest Burgers vectors exist along the [110] direction, which makes it energetically favorable to reconstruct along the (111) slip planes. This dislocation mechanism has been discussed in detail by Finbow et al. The number of atomic layers increases from 16 to 18 beyond the elastic limit. It can be seen from Fig. 2 that alloys having higher composition of Pt require higher stress to bring about slippage along (111) plane and experience this dislocation at higher strains.



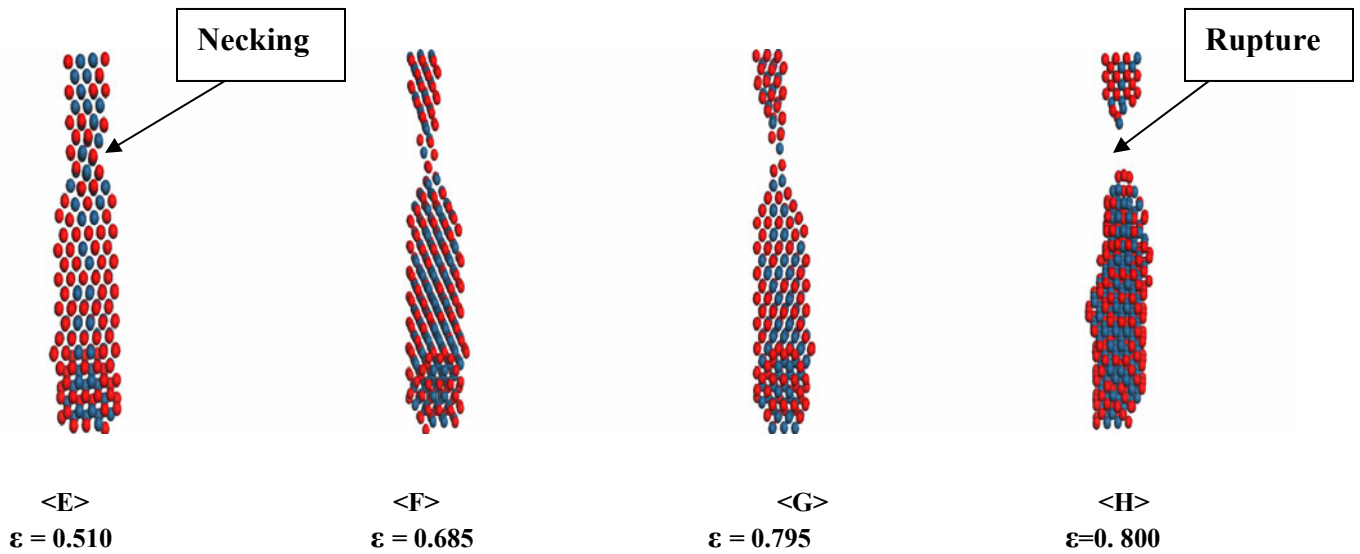


Figure 3. Snapshots showing atomic arrangement of (Pd_{0.5}-Pt_{0.5}) wires at different strain values for T=50 K and strain rate=0.05% ps⁻¹. Pd atoms are represented in red and Pt atoms in blue.

Extension of the re-crystallized nanowires results in a second dislocation to state <D>. A smaller stress (approx. 9.6 GPa for 50% Pt) is required to bring the nanowires to the second dislocation point at $\epsilon=0.125$. In this regime, an out-of-plane rearrangement of atoms along the (111) plane occurs. The reconstructed lattice obtained after the first dislocation is not able to attain the minimum energy state and hence a smaller stress is sufficient to bring about further dislocations. Further increase in strain leads to repetition of the dual process i.e. an elastic stretch followed by a slip. Thus, a series of such dislocations and crystal rearrangement occurs for the subsequent strains. The amount of stress required to bring about subsequent dislocations decreases. During this process, the surface atoms are progressively displaced from their original positions and this leads to surface rupture which results in the neck formation at $\epsilon=0.510$ as shown in <E>. The neck continues to become smaller from <E> to <G> when the two nanowire segments are joined by a mono-atomic strand. The nanowire radius continues to decrease with wire elongation. Once the is sufficiently narrow, i.e. approx. 2**lattice constant*, breaking can take place. This complete rupture occurs at strain value greater than 0.800 for 50% Pt wires as illustrated in <H>.

At low temperatures, the lattice order is highly preserved owing to the smaller atomic oscillations about their equilibrium position. The crystal structure has a tendency to maintain its stable configuration results in well defined periods of yielding. Therefore, the stress-strain response of nanowires at low strain rates and low temperature follows a stepwise periodic behavior in which the nanowire reconstructs, relaxes and subsequently recrystallizes.

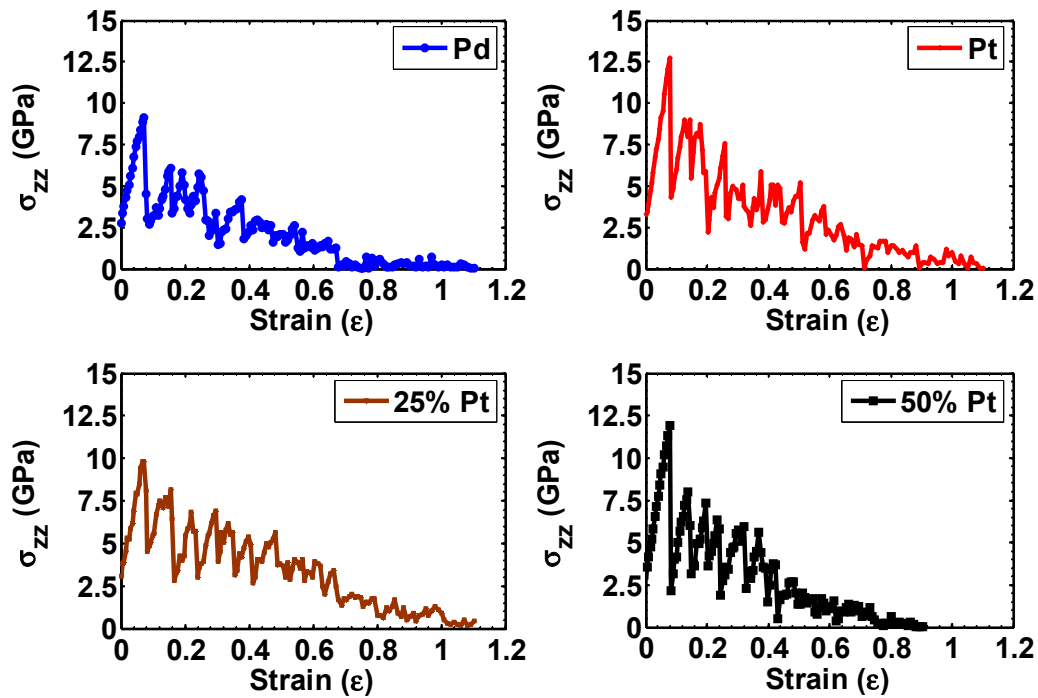
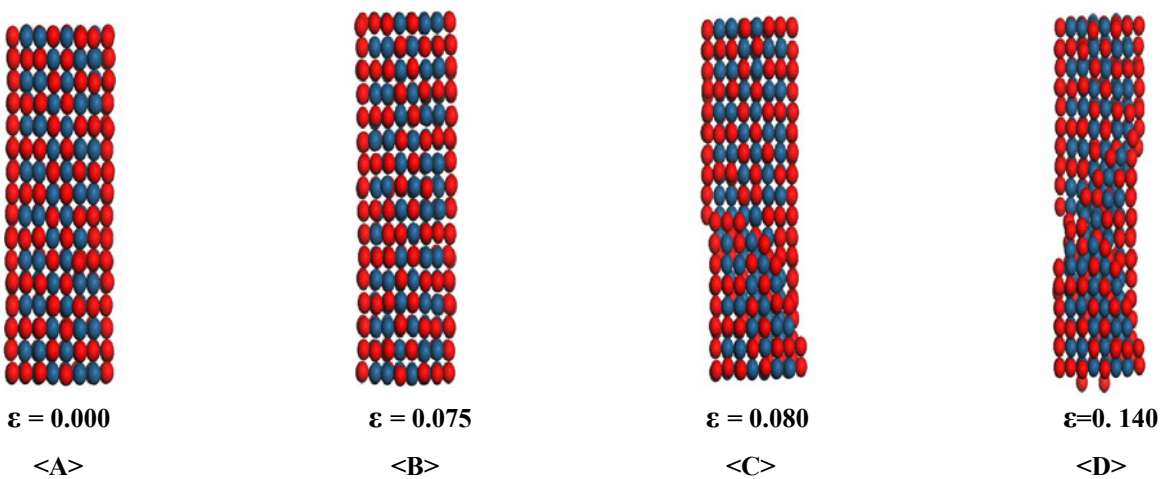


Figure 4. Stress-Strain response of alloy nanowires at $T=300$ K and strain rate= $0.05\%/ps$.

The stress-strain response of transition metal nanowires at 300 K and $0.05\% ps^{-1}$ strain rate is shown in Fig. 4. With an increase in temperature (from 50 to 300 K), the entropy increases and the atoms vibrate about their equilibrium position with increased amplitude. The increased oscillations in turn results in relatively increased lattice instability. As a result, the system favors disruption of lattice order and encourages lattice reconstruction. Therefore, compared to Fig. 2, the nanowires at higher strain rate experience an early onset of slippage. For eg., the 50% Pt nanowire has a 21% lower yield strain (ϵ_{fy}) and a corresponding 20% smaller yield stress (σ_{fy}).



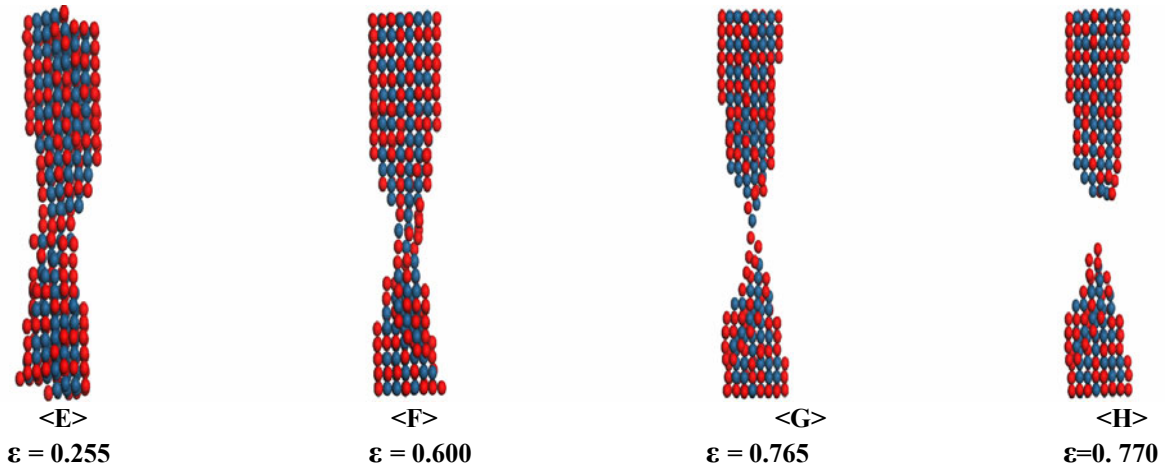


Figure 5. Snapshots showing atomic arrangement of (Pd_{0.5}-Pt_{0.5}) wires at different strain values for T=300 K and strain rate=0.05% ps⁻¹. Pd atoms are represented in red and Pt atoms in blue.

The onset of out-of-plane slippage at 300 K in 50% Pt nanowires occurs earlier at $\epsilon = 0.080$ (<C>), compared to $\epsilon = 0.100$ at 50 K. The periodic slippage and lattice rearrangement continues till surface rupture at $\epsilon = 0.140$. Further increase in strain results in necking observed at $\epsilon_{nc} = 0.255$. The neck continues to become narrower until complete rupture at $\epsilon_{ru} = 0.770$.

The ductility ($\Delta\epsilon_D$) of nanowire is defined as the strain interval between the onset of necking and complete rupture. For 50% Pt alloy at 300 K and 0.05% ps⁻¹, $\Delta\epsilon_D=0.770-0.255=0.515$ or 51.5% whereas the same at 50 K is (0.800-0.510=0.29) or 29%. Therefore, the 50% Pt alloy nanowire at 300 K is about 22% more ductile than at 50 K. The ductility of other metal nanowires is summarized in Table 2. It can be seen that the ductility of nanowires over the entire composition range of Pd increases with increase in temperature. However, at any given temperature, nanowires having 75% Pd composition are more ductile than 50 % Pd alloy as well as mono-metallic wires. It therefore appears that the strain interval between the onset of necking and rupture is influenced by alloy composition as well as the relative strength of the metal-metal interactions. The influence of ductility on nanowire applications is discussed in a subsequent section.

Table 2. Ductility of nanowires at 0.05% strain rate

Nanowire composition (% Pd)	50 K		Ductility (%)	300 K		Ductility (%)
	ϵ_{nc}	ϵ_{ru}		ϵ_{nc}	ϵ_{ru}	
0	0.315	0.610	29.5	0.350	0.910	56
50	0.510	0.800	29	0.255	0.770	51.5
75	0.290	0.775	48.5	0.430	1.050	62
100	0.330	0.670	34	0.250	0.690	44

2. Mechanism of stress-strain response in nanowires under high strain rate conditions.

Under high strain rate conditions ($\dot{\epsilon} = 5\% \text{ ps}^{-1}$), the stress-strain response of nanowires exhibits a completely different behavior as shown in Fig. 6. The stress-strain response of the nanowires exhibits “mini-peaks” or “wavelets” during the yielding cycles, indicative of higher disorder in the crystal lattice. This behavior was observed by Koh et al.⁶ in their simulations of Pt nanowires and by Ikeda et al.¹⁵ for Ni and Cu-Ni alloy nanowires, when subjected to strain rates of up to $4\% \text{ ps}^{-1}$ and $5\% \text{ ps}^{-1}$, respectively. This phenomenon is attributed to the onset of amorphous deformation at higher strain rates. Beyond the first yield strain, the system changes continuously from a crystalline fcc phase to an amorphous phase.

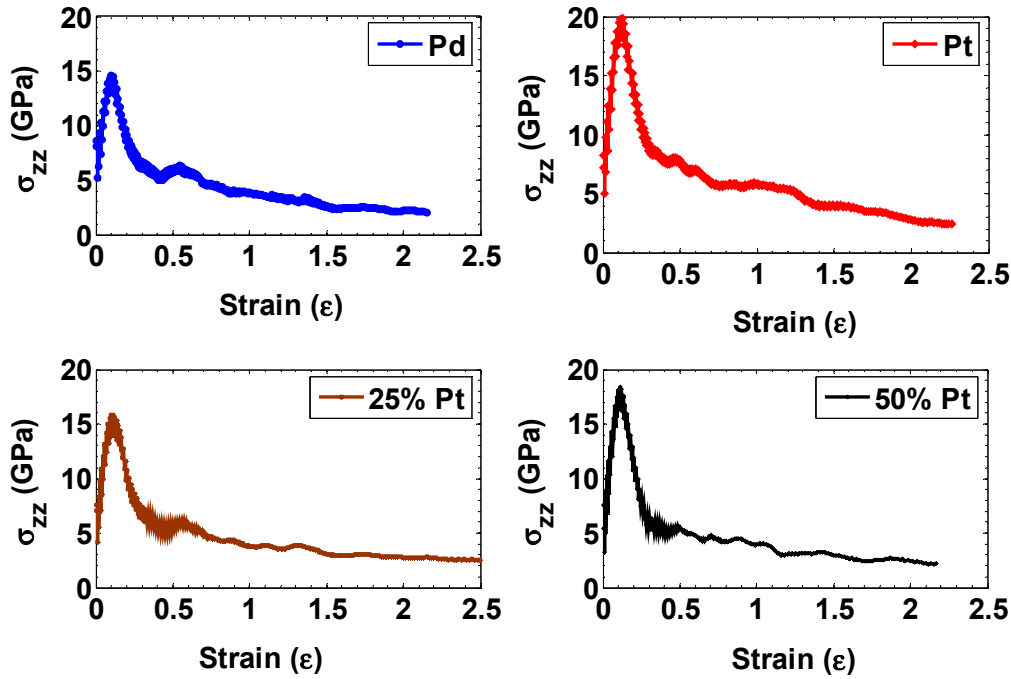


Figure 6. Stress-Strain response of alloy nanowires at $T=50 \text{ K}$ and strain rate= $5\% \text{ ps}^{-1}$.

The onset of amorphous phase at high strain rates is indicated by the snapshots shown in Fig. 7. The slippage allowing for reconstruction along the (111) plane is absent. Instead, the wires exhibit superplasticity behavior right after yielding. Owing to the high degree of lattice disorder, the nanowires yield at extremely high stresses. For 50% Pd nanowires, the yield stress (σ_{fy}) corresponds to 18.4 GPa and corresponding yield strain (ϵ_{fy}) of 0.110 at 50 K. The stress required at 50 K is 22 % higher and the corresponding strain is 16% higher than that required at $\dot{\epsilon}=0.05\% \text{ ps}^{-1}$. Beyond this strain, the deformation of nanowire proceeds uniformly with no necking phenomenon observed for all the wires. The nanowires continue to extend and experience complete rupture at extremely higher strains. The rupture strain (ϵ_{ru}) is 2.10 for 50 % Pd nanowire.

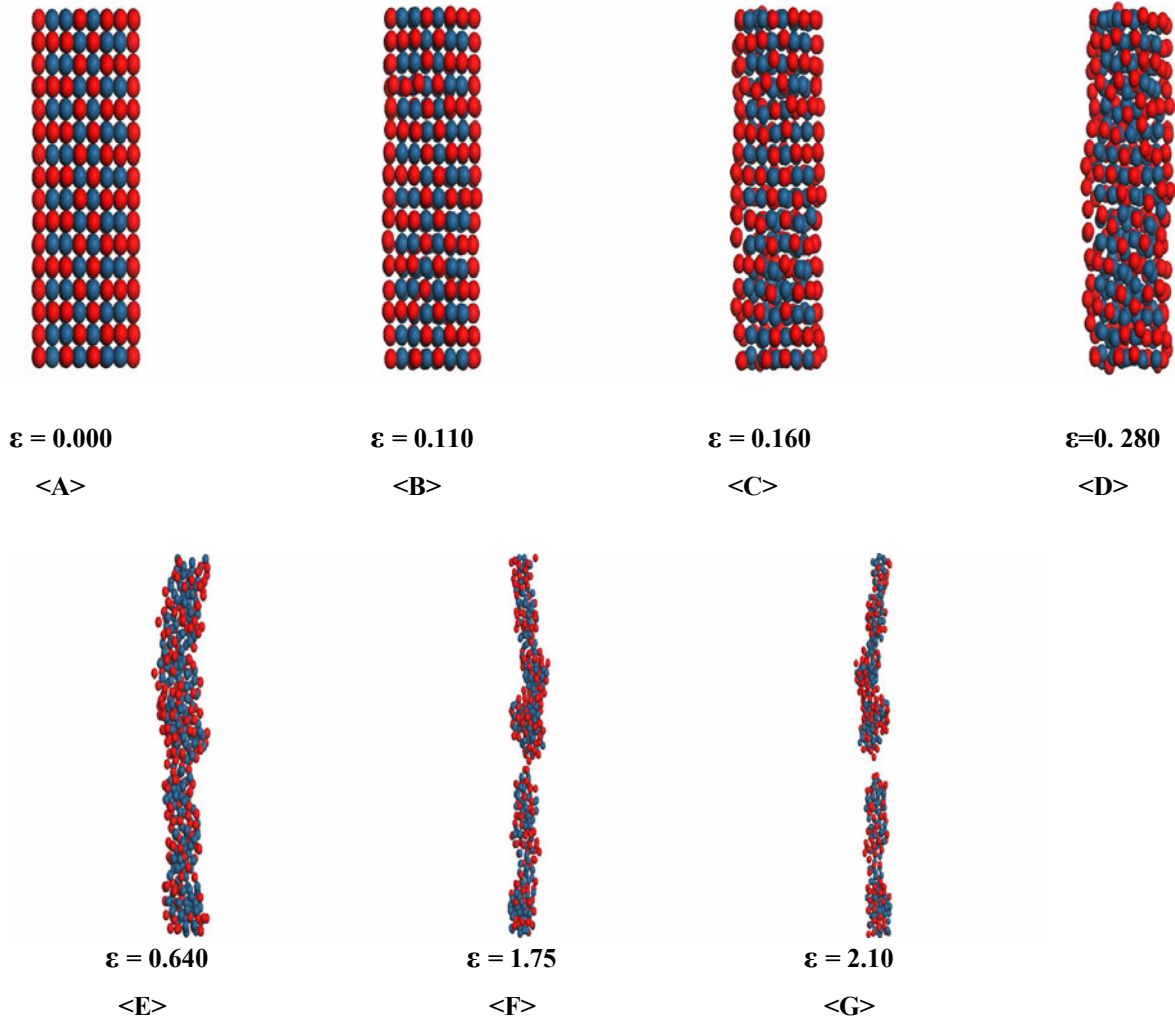


Figure 7. Snapshots showing atomic arrangement of (Pd_{0.5}-Pt_{0.5}) wires at different strain values. Pd atoms are represented in red and Pt atoms in blue.

The extension of nanowires at higher strain rate appears to be associated with structural changes. From the snapshots shown in Fig. 7, the nanowires appear to be evolving into a helical structure. The existence of helical structures in Pt nanowires was reported in the simulations of Koh et al.⁶ However, at the strain rates simulated by them, the formation occurred at the junction of the two nanowire segments before complete rupture. In our case, the nanowire appears to be evolving into stable helical structures along its entire length. It appears that at the extremely high aspect ratios, the fcc structure might not represent the most stable phase and therefore the amorphous/melted material would transform into a multi-shelled helix. Indeed, such a structure has been reported to occur for Pt nanowires by Oshima et al.¹⁶ who used electron beam thinning method at elevated temperatures to form 6-0 single walled platinum nanotube having approx. 0.48 nm diameter. It is possible that the mechanical extension of fcc nanowires at 50 K and $\dot{\varepsilon} = 5\% \text{ ps}^{-1}$ might have led to the formation of similar helical structure observed by Oshima et al. Depending on the alloy composition, a residual stress of about 2.5-3 GPa was observed after the rupture of the nanowire into its fragments. This could be attributed to the presence of stable structures (possibly helical) within the broken fragments or else be an artifact of the long range nature of the potential, which would give rise to a detectable force between the separated portions of the wire. This would however require a separate investigation of its own.

3. Structural analysis

Radial distribution function (RDF) can be used to analyze the structural changes associated with the different strain rates. RDF of $(\text{Pd}_{0.5}\text{-Pt}_{0.5})$ nanowire strained along the $[001]$ direction at 50 K and low strain rates is shown in Fig. 10. The crystalline fcc structure is indicated by the RDF of nanowires at $\epsilon=0$. With an increase in strain the peak value of the nearest neighbor distance is reduced. Further splitting in the peaks is also observed. The phenomenon responsible for splitting of the peaks is illustrated in Fig. 9. Upon elongation to $\epsilon=0.09$, the nearest neighbor distances along the (001) plane is reduced whereas the nearest distances along the (100) plane increases leading to a face centered orthorhombic structure as shown in Fig. 9. The corresponding distributions of the first neighbor distances are therefore split into the two peaks, each peak representative of the nearest neighbor distance along the (100) and (001) plane, respectively. Further stretching of the nanowires beyond the first yield (ϵ_{fy}) results in a crystal rearrangement back to an fcc structure as shown in Fig. 10. The number of atomic layers increases from 16 to 18 to compensate for the increase in length while maintaining the inter-atomic distance of 2.75 \AA .

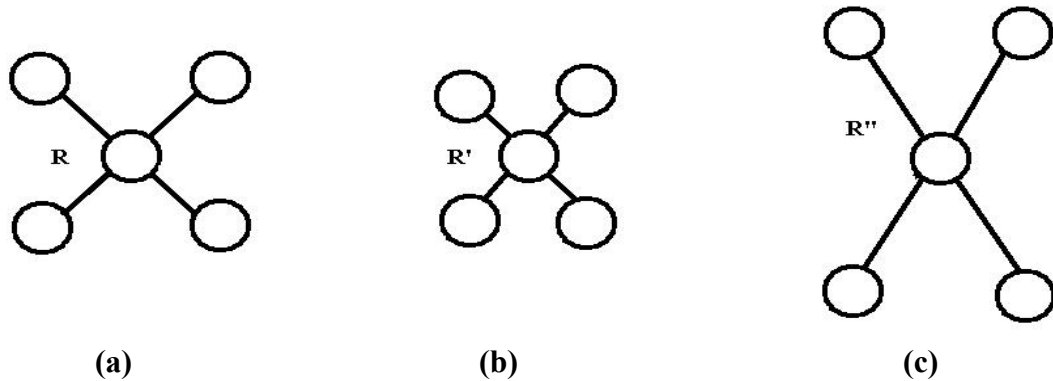


Figure 8. During elastic deformation, FCC evolves into a FCO (face centered orthorhombic) structure. The initial fcc structure with radius R at zero strain is shown in (a). When subjected to a tensile strain along the $[001]$ direction, the nearest neighbor distances change as $R'' > R > R'$. Along the (001) plane, the inter-atomic distance in nanowires reduces as shown in (b), whereas they increase along the (100) plane as shown in (c).

When subjected to higher strain rate ($5\% \text{ ps}^{-1}$), the first peak in the nanowire RDF broadens whereas the second peak located at $\sim 0.38 \text{ nm}$ and representing the octahedral sites gradually disappears as the strain increases beyond $\epsilon=0.11$ (shown in Fig. 9). The nanowire structure transforms homogeneously from an original crystalline FCC structure to the amorphous state with no evidence of stress hardening or necking that is observed in metal nanowires at lower strain rates. At higher strain rates, the atoms do not have sufficient time to diffuse and form a stable crystalline configuration corresponding to the physical configuration with lower energy. Similar behavior is also exhibited by Ni, Au and NiCu nanowire when subjected to high strain rates ($5\text{-}15\% \text{ ps}^{-1}$).

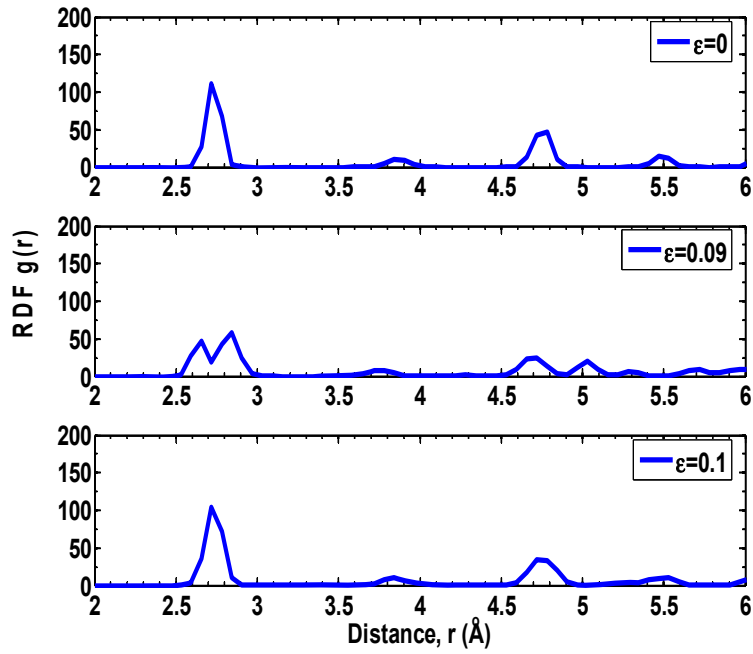


Figure 9. Radial distribution function of nanowire strained along the [001] direction at 50 K and $0.05\% \text{ ps}^{-1}$.

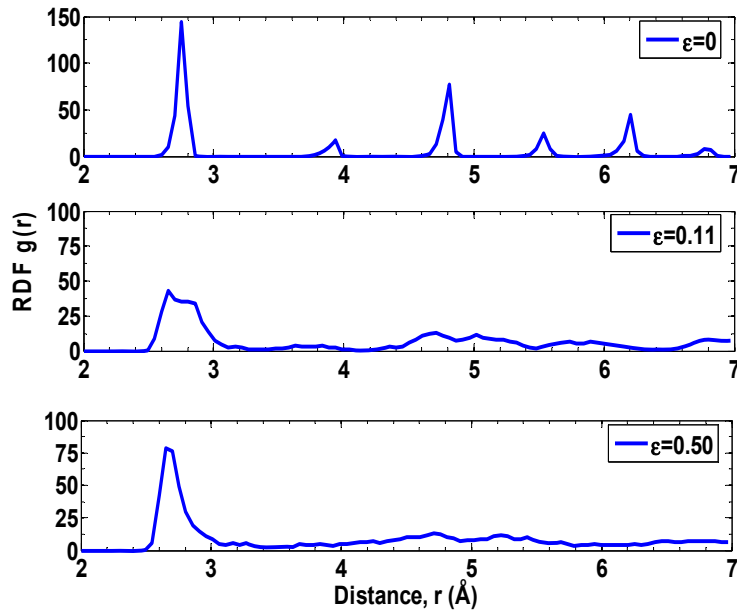


Figure 10. Radial distribution function of nanowire strained along the [001] direction at 50 K and $5\% \text{ ps}^{-1}$.

4. Calculation of elastic properties of nanowires

The Young's modulus and Poisson ratio are computed for the different nanowires prior to the first yield strain at the respective temperature and strain rates. A linear regression analysis of the scatter plots of

stress-strain data was used to obtain the least squares best fit straight line through sample points. The slope of the line gave the Young's modulus under various loading conditions. A correlation coefficient (r) was used to quantify the degree of linearity between the stress and strain data points. Physically, it is indicative of the stability of the lattice when subjected to axial deformation. Higher the value of the correlation coefficient, the more stable is the crystal lattice. At $r=100\%$, the constituent atoms do not vibrate about its equilibrium position (eg. Lattice structure at $T=0$ K) whereas at $r=0\%$ the system is in maximum entropy state and is indicative of a completely random cluster with the atoms exhibiting Brownian motion (rare gases). The Young's modulus and the associated correlation coefficient are summarized in Table 3.

Table 3. Young's modulus (GPa) of various nanowires under different loading conditions

Nanowire	Property	$\dot{\epsilon} = 0.05\% \text{ ps}^{-1}$		$\dot{\epsilon} = 5\% \text{ ps}^{-1}$	
		50 K	300 K	50 K	300 K
Pd	E	105	89.8	82	IN PROGRESS
	r (%)	99.75	99.73	83.29	IN PROGRESS
Pd _{0.75} -Pt _{0.25}	E	120	97	104	IN PROGRESS
	r (%)	99.97	99.35	84.32	IN PROGRESS
Pd _{0.5} -Pt _{0.5}	E	130	117	134	IN PROGRESS
	r (%)	99.78	99.74	85.64	IN PROGRESS
Pt	E	152	126	135	IN PROGRESS
	r (%)	99.96	99.72	89.94	IN PROGRESS

The bulk value of Young's modulus for Pd and Pt are 121 and 168 GPa, respectively. At low strain rates, the Young's modulus for the nanowires is at least 25% lower at 300 K and 10% (for Pd) - 14% (for Pt) lower at 50 K. At high strain rates and 50 K, the elastic modulus is 32% (for Pd) and 20% (for Pt) lower than respective bulk values. The correlation between the stress and the strain values is above 99% and is therefore very strong at lower strain rates. At high strain rates, the nanowire experiences higher degree of disorder. The onset of amorphous phase results in significant lowering of the correlation coefficients, even at temperatures as low as 50 K as shown in Table 3. Therefore, nanowires when subjected to higher strain rates are significantly softened as also indicated by the Young's modulus. The implications of a lesser stiff nanowire on their applicability in MEMS and other areas are discussed in a subsequent section.

The Poisson ratio was calculated following a similar procedure by carrying out a regression analysis on a scatter plot of radial (ϵ_{rr}) vs. axial strain (ϵ_{zz}). The radial strain of the nanowire is defined as $\epsilon_{rr} = \frac{R - R_i}{R_i}$, where R is the radius of the wire at strain state ϵ_{zz} , and R_i is the initial radius of the nanowires in their unstressed state. The mean distance of the surface atoms from the centroid of nanowire was used to obtain the average radius R at each strain state. Figure 12 shows the determination of Poisson ratio from a plot of axial vs. lateral strain for one particular case. The results for different loadings are summarized in Table 4.

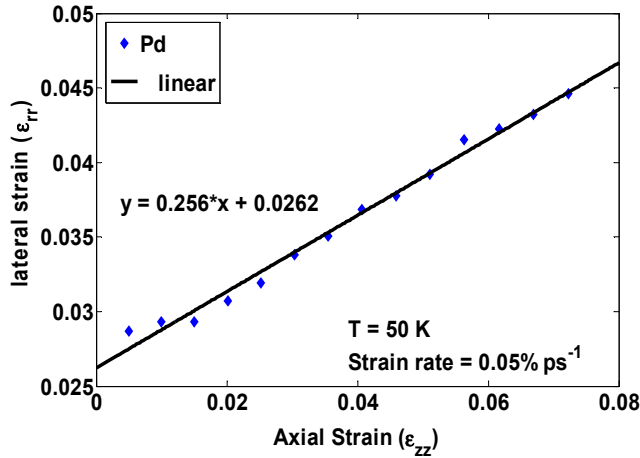


Figure 11. Determination of Poisson ratio for Pd nanowire at T=50 K and $\dot{\epsilon} = 5\% \text{ ps}^{-1}$.

The Poisson ratio for bulk Pd and Pt correspond to 0.38 and 0.39, respectively. The Poisson ratios of Pd-Pt alloys have values between 0.38 and 0.39. At the nanoscale, the Poisson ratios of Pd and Pd rich alloys vary significantly from bulk values. The Poisson ratio of Pd and 25% Pt alloy nanowires are 32% and 21% lower than bulk. The Poisson ratio of most materials lies between 0 and 1. Materials with Poisson ratio 0.5 (eg. rubber) are considered incompressible. The lower value of Poisson ratio suggests that the material is more compressible. Pd and Pd rich alloys are therefore more compressible and malleable than Pt and Pt rich alloys.

Table 4. Poisson ratio (ν) of nanowires for different loading conditions

Nanowire	Property	$\dot{\epsilon} = 0.05\% \text{ ps}^{-1}$		$\dot{\epsilon} = 5\% \text{ ps}^{-1}$	
		50 K	300 K	50 K	300 K
Pd	ν	0.26	0.23	0.27	IN PROGRESS
	r (%)	99.46	95.21	88.17	IN PROGRESS
	ν	0.30	0.28	0.28	IN PROGRESS

Pd_{0.75}-Pt_{0.25}	r (%)	99.24	98.07	89.34	IN PROGRESS
Pd_{0.5}-Pt_{0.5}	v	0.32	0.30	0.29	IN PROGRESS
	r (%)	99.66	97.75	91.38	IN PROGRESS
Pt	v	0.35	0.34	0.34	IN PROGRESS
	r (%)	99.79	98.02	97.16	IN PROGRESS

At low strain rates and high temperatures such as 300 K, the Poisson ratio of nanowires is 3-13% lower than at low temperature i.e. 50 K depending on the alloy composition. The slightly higher compressibility is attributed to the increased kinetic energy at higher temperature. With increase in strain rates, onset of amorphous transformation takes place and there is a further reduction in the Poisson ratio of nanowires. The higher malleability is attributed to increased lattice disorder. The increase in crystal ductility as well as malleability and compressibility, results from the development of short ranged order of the crystal structure at higher strain rates. The Poisson ratio and other mechanical properties of (Pd_{0.5}-Pt_{0.5}) nanowires are summarized in Table 4. The influence of the various derived mechanical properties of nanowires on their applicability in sensing and other applications is discussed in a subsequent section.

Table 5. Summary of mechanical properties of (Pd_{0.5}-Pt_{0.5}) nanowires

Nanowire property		$\dot{\epsilon} = 0.05\% \text{ ps}^{-1}$		$\dot{\epsilon} = 5\% \text{ ps}^{-1}$	
		50 K	300 K	50 K	300 K
First Yield	Strain	0.095	0.075	0.110	IN PROGRESS
	Stress (GPa)	15.03	11.90	18.38	IN PROGRESS
Rupture		0.800	0.770	2.10	IN PROGRESS
Ductility		29	51.5	146	IN PROGRESS
Young's Modulus		130	117	134	IN PROGRESS
Poisson ratio		0.32	0.30	0.29	IN PROGRESS

V. Discussion

Pd and its alloy nanomaterials find applications in sensing and catalysis. The nanomaterial sensing layers are utilized in surface acoustic wave (SAW) devices to detect chemical and biological species. The elastic properties of these nanowires play a significant role in determining the device sensitivity and speed of response.

The Young's modulus as well as the Poisson's ratio of a material influences the speed of propagation and reflection of surface acoustic waves. In sensing applications, the ratio of compressional to shear wave speed is important in inferring the device sensitivity and speed of response. This wave speed ratio depends on Poisson's ratio. Poisson's ratio also affects the decay of stress with distance, and the distribution of stress.

Comparisons of finite element simulations of a typical SAW gas sensor (100 MHz) utilizing a Pd nanomaterial sensing layer with properties derived from the present study and a thin Pd film have shown significant differences in the wave propagation velocities. Our simulations (ignoring any mass loading effect) indicate a time delay of 1 ns in the acoustic wave propagation between the two cases which is attributed to changes in elastic modulus. Experimental studies by Srinivasan et al. have also shown significant differences in the sensitivity and speed of response of SAW sensor devices utilizing nanomaterials which cannot be solely explained on the basis of increased surface area. Although the mechanical properties of nanowires in gaseous and liquid environment are required to quantitatively establish the sensor characteristics, the present results do indicate that significant differences between the nanoscale and bulk elastic properties prevail which are likely to have a bearing on the applications of nanowires as sensing layers in gas and biological sensors.

VI. Conclusions

Molecular dynamics simulation of Pd, Pt and Pd-Pt alloy nanowires subjected to a uniaxial tensile strain along the [001] direction was investigated. The changes in the crystal structure and mechanical properties of nanowires under various loading conditions were analyzed. It was observed that the crystalline order is maintained at low strain rates and periodic elastic yielding cycles were observed with planar dislocation and slippage occurring along the (111) plane. The deformation behavior at low temperatures such as 50 K is characterized by brittle slips and rupture with low ductility. On elongation within the first yield, the analysis of RDF reveals that the initial fcc crystal structure changes into face centered orthorhombic (fco) type. Alloys richer in Pt composition required higher applied stresses before yielding and yield at higher strains than alloys having lower Pt. With an increase in temperature for the same applied strain rate, the system entropy increases and periodic response of the nanowires becomes less defined. The ductility of nanowires increases with temperature over the entire range of Pd composition.

The stress-strain response at high strain rates is less strongly correlated. An increase in strain rate at 50 K results in a continuous change from crystalline to amorphous type for all the nanowires, thereby displaying superplasticity behavior. The amorphous nanowire appears to re-crystallize into a relative stable single walled helical structure. The helical structure increases the ductility of the nanowires. It remains to be seen whether the helical structure occurs and/or remains stable at high temperature and strain rates. Efforts are underway to simulate the same. The complete rupture occurs when the wire length is approximately three times its original length.

At the nanoscale, the calculated Young's modulus and Poisson ratio depend on the applied strain rate which is a characteristic of viscoelastic materials. It was found that the Young's modulus of nanowires is about 70-85% of the bulk value with the exact lowering dependant on the alloy composition. Similarly, the Poisson ratio of Pd rich alloys is 60-70% of its bulk value whereas that of Pt rich alloys is not significantly changed at the nanoscale. The differences in elastic properties are attributed to the finite size effect. The effect of the differences in mechanical properties of nanowires on their applicability in sensing is discussed. The current findings have laid groundwork for further investigations into other aspects of mechanical

properties such as axial compression and bending. The results from the present study can also be used as input for linear continuum modeling involving nanostructures such as Pd, Pt and its alloys.

Acknowledgement:

Partial support was provided by NASA-GRC. The Daresbury laboratory provided the DL_POLY package and the Research Computing Core Facility at the University of South Florida provided the computational resources, both of which are gratefully acknowledged. One of the authors (SKRSS) also wishes to thank Reetu Singh for useful discussions.

References:

- 1 W. Liang and M. Zhou, *J. Eng. Mater. Technol.* **127**, 423 (2005).
- 2 W. Liang, M. Zhou, and F. Ke, *Nano Lett.* **5**, 2039 (2005).
- 3 K. Gall, J. Diao, and M. L. Dunn, *Nano Lett.* **4**, 2431 (2004).
- 4 H. S. Park and J. A. Zimmerman, *Physical Review B: Condensed Matter and Materials Physics* **72**, 054106/1 (2005).
- 5 H. S. Park, K. Gall, and J. A. Zimmerman, *Journal of the Mechanics and Physics of Solids* **54**, 1862 (2006).
- 6 S. J. A. Koh, H. P. Lee, C. Lu, and Q. H. Cheng, *Physical Review B: Condensed Matter and Materials Physics* **72**, 085414/1 (2005).
- 7 W. Bin, A. Heidelberg, and J. J. Boland, *Nature materials* **4**, 525 (2005).
- 8 D.-L. Chen and T.-C. Chen, *Nanotechnology* **16**, 2972 (2005).
- 9 J.-S. Lin, S.-P. Ju, and W.-J. Lee, *Physical Review B: Condensed Matter and Materials Physics* **72**, 085448/1 (2005).
- 10 J. Diao, K. Gall, and M. L. Dunn, *Nat. Mater.* **2**, 656 (2003).
- 11 J. Diao, K. Gall, and M. L. Dunn, *Nano Lett.* **4**, 1863 (2004).
- 12 H. S. Park, *Nano letters* **6**, 958 (2006).
- 13 H. S. Park, K. Gall, and J. A. Zimmerman, *Physical Review Letters* **95**, 255504/1 (2005).
- 14 J. C. Gonzalez, V. Rodrigues, J. Bettini, L. G. C. Rego, A. R. Rocha, P. Z. Coura, S. O. Dantas, F. Sato, D. S. Galvao, and D. Ugarte, *Physical Review Letters* **93**, 126103/1 (2004).
- 15 H. Ikeda, Y. Qi, T. Cagin, K. Samwer, W. L. Johnson, and W. A. Goddard, III., *Physical Review Letters* **82**, 2900 (1999).
- 16 Y. Oshima, H. Koizumi, K. Mouri, H. Hirayama, K. Takayanagi, and Y. Kondo, *Physical Review B: Condensed Matter and Materials Physics* **65**, 121401/1 (2002).